Journal of Molecular Structure 1340 (2025) 142497

Contents lists available at ScienceDirect

Journal of Molecular Structure

journal homepage: www.elsevier.com/locate/molstr

Rating of *in vitro* cytotoxicity activities and anti-xanthine oxidase activities of some non-proteoneogenic amino acid derivatives by molecular docking and molecular dynamics studies

Zuhal Alım [a,*], Serap Yalçın Azarkan [b], Namık Kılınç [c], Ebru Akkemik [d]

[a] Department of Chemistry, Faculty of Arts and Sciences, Kırşehir Ahi Evran University, Kırşehir 40100, Türkiye
[b] Department of Medical Pharmacology, Faculty of Medicine, Kırşehir Ahi Evran University, Kirsehir 40100, Türkiye
[c] Department of Medical Services and Techniques, Vocational School of Health Services, Iğdır University, Iğdır 76000, Türkiye
[d] Department of Food Engineering, Faculty of Engineering, Siirt University, Siirt 56100, Türkiye

ARTICLE INFO

Keywords:
Xanthine oxidase
Inhibition
Breast cancer
Cytotoxicity
Molecular docking

ABSTRACT

Hyperuricemia is a chronic disease closely associated with many pathological conditions, including cancer, which occur due to increased uric acid levels. Xanthine Oxidase (XO) facilitates the stepwise conversion of hypoxanthine to xanthine and subsequently to uric acid, serving a crucial function in purine metabolism. XO inhibitors are the most important therapeutic agents for the control of hyperuricemia. The fact that existing XO inhibitors have serious side effects has made it necessary to describe original, impressive inhibitors with minor side effects. In this study, since the close relationship between hyperuricemia and cancer, the inhibition effects of some non-proteogenic amino acid derivatives (1-4) on XO activity and their cytotoxic effects on triple-negative breast cancer cell line (MDA-MB-231) were examined together. The inhibition effects of molecules **1-4** on XO activity were determined by IC_{50} values, and for XO, IC_{50} values of **1-4** were found to be 1.338 μM, 1.357 μM, 1.788 μM, 1.228 μM respectively. The cytotoxic effect of the molecules (**1-4**) on MDA-MB-231 cell lines was investigated by XTT analysis. According to the results obtained, it is seen that the effect of the **2**nd (IC_{50}:98.55 μM) molecule is more toxic on the cells than the others and molecule **2** demonstrated significant inhibition of cell migration in MDA-MB-231 cells in a compared to the untreated control. The study was supported by molecular docking and molecular dynamics and ADME analyses. In conclusion, the results of this study may be useful in the design of XO inhibitor drugs for the treatment of hyperuricemia by contributing to the synthesis of new, effective amino acid-derived XO inhibitors with fewer side effects.

1. Introduction

Hyperuricemia (HUA) is a chronic disease associated with increased uric acid levels resulting from catabolic reactions of purine nucleotides. HUA is clinically defined as serum uric acid (SUA) levels exceeding 420 μmol/L in men and 360 μmol/L in women [1]. HUA causes gout, an inflammatory arthritis caused by the accumulation of uric acid crystals, especially in the joints [2]. Moreover, HUA is linked to a wide range of acute and chronic conditions, including coronary heart disease, tumor lysis syndrome, and renal failure. It is also implicated in arterial hypertension, hemospermia, and metabolic syndrome [3–5]. Additionally, HUA contributes to circulatory shock, ischemia-reperfusion injury, and vascular complications associated with diabetes. Furthermore, it plays a role in cancer progression, adipogenesis [6,7], and other systemic disorders, highlighting its broad pathological significance. Elevated uric acid levels can contribute to systemic inflammation and oxidative stress, which may cause damage to tissues. This heightened inflammation and oxidative stress can diminish the protective antioxidant effects of uric acid, potentially promoting tumor formation, growth, and metastasis. High uric acid levels might significantly influence cancer progression by mediating signaling pathways in adipose tissue, leukocytes, and cancer cells, primarily through inflammatory mechanisms [8]. The prevalence of HUA and HUA-related diseases has been increasing worldwide in recent years [9]. Therefore, it is very important to identify effective drugs for the treatment of HUA, and Xanthine Oxidase (XO) inhibitors are molecules that are central to drug development studies for the control of hyperuricemia [9]. XO is a crucial metalloenzyme that facilitates the oxidative hydroxylation of hypoxanthine to xanthine and then

* Corresponding author.
E-mail address: zuhal.alim@ahievran.edu.tr (Z. Alım).

https://doi.org/10.1016/j.molstruc.2025.142497
Received 9 July 2024; Received in revised form 14 March 2025; Accepted 25 April 2025
Available online 26 April 2025

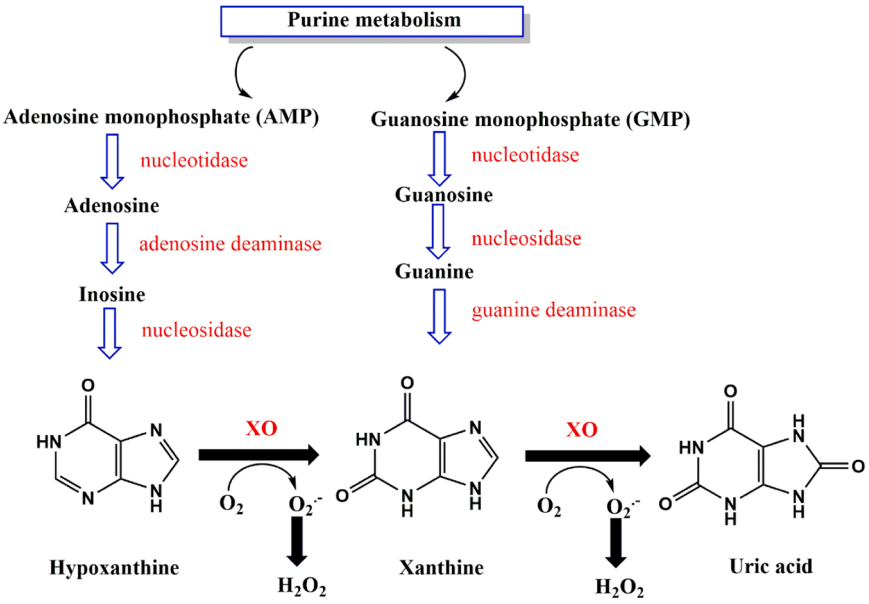

Fig. 1. Purine catabolism and uric acid genaration.

xanthine to uric acid during the final stages of purine metabolism [10] (Fig. 1). As a result of this reaction catalyzed by XO, high amounts of superoxide radicals and hydrogen peroxide (H_2O_2) are formed along with the formation of uric acid. Excessive activity of XO not only causes hyperuricemia, but also results in the formation of reactive oxygen species such as superoxide radical and hydrogen peroxide. Therefore, the XO enzyme is an important source of oxidative stress in the vascular system [11,12]. This situation leads to many pathological conditions. Disrupted XO activity triggers free radical-driven neurotoxicity, leading to cellular damage and inflammatory responses. Research has established a direct link between heightened XO activity and mental disorders like schizophrenia and depression [13]. It has also been reported that the prevalence of Metabolic Syndrome (MS) is high in gout patients [14]. It is known that circulating XO is also increased in hemolytic diseases such as sickle cell, malaria and sepsis [15]. On the other hand, hyperuricemia is associated with increased cancer incidence and cancer-related deaths [16], and excess ROS produced as a result of the reaction catalyzed by XO induces stages of tumor progression such as tumor cell proliferation, angiogenesis, cell migration and incursion in the case of cancer, therefore XO inhibitors also are potential therapeutic agents for cancer treatment [17].

Xanthine oxidase inhibitors reduce both uric acid levels and oxidative stress in the vascular system [9]. Therefore, to date, A number of XO inhibitors have been identified such as oxypurinol, febuxostat,

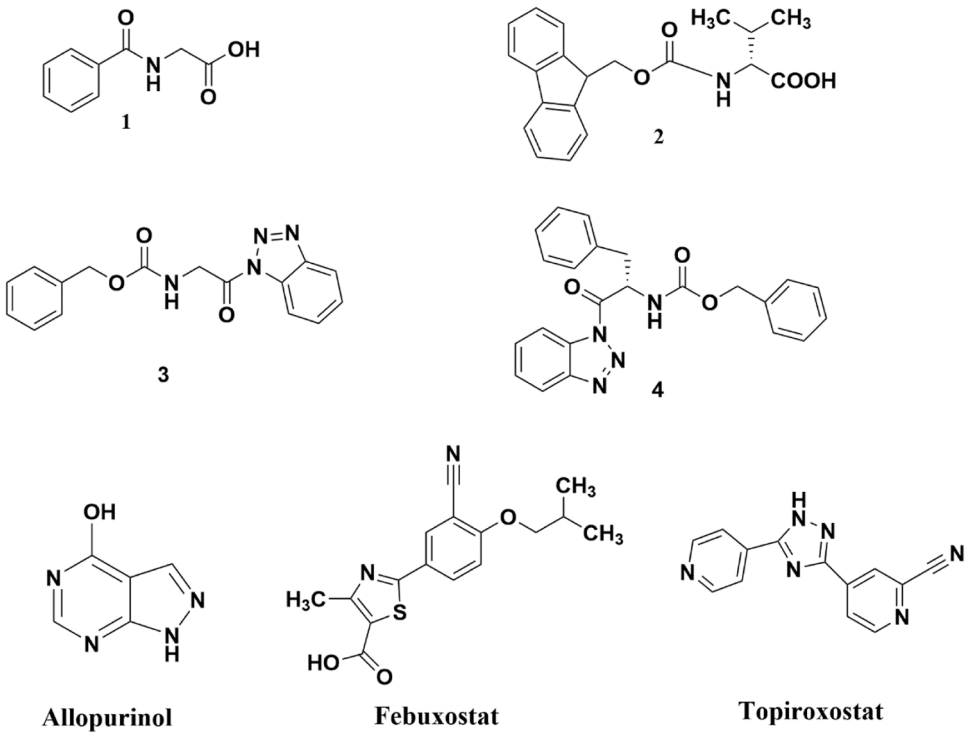

Fig. 2. Chemical structure of the non-proteinogenic amino acid compounds (**1, 2, 3** and **4**) used in this study and structure of known XO inhibitors.

allopurinol, topiroxostat [18], pegloticase, sulfinpyrazone, BCX4208, probenecid, etc. for the treatment of hyperuricemia disorders [3,19,20]. Of these inhibitors, only allopurinol, which is a purine derivative, and febuxostat and topiroxostat, which are not purine derivatives, are approved for the treatment of hyperuricemia and gout [21]. Despite its long-standing clinical use for over five decades in treating hyperuricemia and gout, allopurinol and its active metabolite, oxypurinol, are linked to severe adverse effects, including skin rashes, hypersensitivity reactions, gastrointestinal distress, nephrotoxicity, and eosinophilia [21–24]. Additionally, febuxostat was determined to have higher cardiovascular mortality than allopurinol and was required to receive a black box warning label by the FDA in February 2019 [21,25,26]. Conversely, side effects such as liver dysfunction [27,28], gouty arthritis, and skin rash [27] have been reported with topiroxostat. Due to the serious side effects of XO inhibitors designated for the treatment of hyperuricemia, treating hyperuricemia and gout without any adverse effects is still a challenge for pharmaceutical industries. This has led to the need to develop new non-purine derivative XO inhibitors that are more forceful and have minor side effects for the treatment of hyperuricemia and gout [29].

Amino acid derivatives are widely used as enzyme inhibitors in the field of medicinal chemistry and new drug discovery studies due to their diversity of biological activities, ease of synthesis of side chains, and chiral properties [30–34]. Peptides and proteins hold a pivotal role in modern drug discovery for their facile synthesis, minimal toxicity, and precise target selectivity. However, their therapeutic potential is constrained by objections such as low bioavailability and limited stability. To overcome these impediments, non-proteogenic amino acids (NPAAs), which are not encoded in the human genome, have become valuable tools to enhance structural diversity and improve pharmacokinetics [35]. In this study, the inhibitory effects of some non-proteinogenic amino acid compounds (hippuric acid (**1**), *N*-(9-Fluorenylmethoxycarbonyl)-D-valine (**2**), *N*-Z-(1-Benzotriazolylcarbonyl) methylamine (**3**), (S)-N-Z-1-Benzotriazolylcarbonyl-2-phenylethylamine (**4**)) (Fig. 2) on XO activity were investigated. Allopurinol was used as the reference inhibitor. Molecular docking and molecular dynamics simulation studies were performed for these amino acid derivatives that have an inhibitory effect on xanthine oxidase activity. In addition, the cytotoxic effect of these non-proteogenic amino acid derivatives (**1-4**) on triple-negative breast cancer cells line (MDA-MB-231) was investigated and ADME analyzes of the molecules were performed. The MDA-MB-231 cell line, originating from the pleural effusion of a patient with invasive ductal carcinoma at MD Anderson, is a widely used model for advanced breast cancer research [36]. Characterized by its high aggressiveness and invasiveness, MDA-MB-231 is extensively studied in both *in vitro* and *in vivo* settings, demonstrating only a moderate response to chemotherapy [36,37].

2. Materials and method

2.1. Materials

All chemicals, amino acid compounds (For compound **1**: CAS No. 495-69-2, purity: 98 %), for compound **2**: CAS No. 84624-17-9, purity: ≥98.0 %, for compound **3**: CAS No. 173459-80-8, purity: >98 %, for compound **4**: CAS No. 769922-77-2, purity: 98 %), bovine milk xanthine oxidase (CAS No. 9002-17-9) and allopurinol (CAS No.315-30-0, quality level: 300) used in this research were commercially available from Sigma-Aldrich Co. (Sigma-Aldrich Chemie GmbH, Germany). Spectrophotometer (THERMO, GENESYS 10S UV-VIS) was used in inhibition studies and ELISA Reader (BIOTEK, USA) was used in cytotoxicity studies.

2.2. Inhibition studies on XO

Xanthine oxidase activity was assessed using a method adapted from Massey et al. [38]. The reaction tracked xanthine oxidation to uric acid by measuring absorbance increase at 295 nm within a 1 mL assay mixture containing 50 mM Tris-HCl buffer (pH 7.6) and 0.1 mM xanthine, equilibrated with air at 25 °C. The extinction coefficient difference between xanthine and uric acid at 295 nm was set at 9.6×10^3 $M^{-1} \cdot cm^{-1}$. Enzyme activity was quantified in micromoles of xanthine converted to uric acid per minute. The inhibitory effects of **1, 2, 3, 4** compounds and allopurinol on xanthine oxidase activity were determined by measuring at least five different concentrations of these compounds (For compound **1**: 0.160 μM, 0.961 μM, 1.602 μM, 1.923 μM, 2.243 μM, for compound **2**: 0.0736 μM, 0.736 μM, 1.104 μM, 1.472 μM, 1.656 μM, for compound **3**: 0.451 μM, 1.353 μM, 1.804 μM, 2.029 μM, 2.255 μM, for compound **4**: 0.212 μM, 0.424 μM, 0.848 μM, 1.272 μM, 1.696 μM, for allopurinol: 0.404 μM, 0.606 μM, 1.616 μM, 2.424 μM, 2.828 μM. These five different concentrations were determined by preliminary experiments with concentration scans. Measurements at each concentration were repeated three times. As a result of each measurement, the enzyme unit was calculated. Enzyme activity without inhibitor was used as a control and %Activity was accepted as 100. Then, enzyme units with inhibitors were calculated for each compound and % Activity values were determined from there. Inhibitor concentrations versus %Activity were graphed, and from these graphs, the inhibitor concentrations that halved the control activity of the enzyme, that is, IC_{50} values, were determined. The same procedures were performed for the reference inhibitor Allopurinol.

2.3. Preperation of cell culture

MDA-MB-231 triple-negative breast cancer cells and MCF-10A normal breast epithelial cells utilized in this study were obtained from the American Type Culture Collection (ATCC). The cancer cells were maintained in RPMI 1640 medium, enriched with 10 % fetal bovine serum and gentamycin antibiotics, under a humidified 5 % CO_2 atmosphere at 37 °C. MCF-10A cells were cultured in DMEM/F-12 medium supplemented with 5 % (v/v) horse serum, 10 μg/mL human insulin, 20 ng/mL hEGF, 100 ng/mL cholera toxin, and 0.5 μg/mL hydrocortisone.

2.4. Cytotoxicity analysis on MDA-MB-231 and MCF-10A cell line

Cytotoxicity analysis was performed on the MDA-MB-231 and MCF-10A cell line to determine the cytotoxic effect of the **1-4** molecules. The different doses were calculated for the molecules (**1-4**) were administered to the cells in a well plate in serial dilutions starting from 1000 μM. In all examples, the highest dose was applied to the cells as 1000 μM in the first stage of the study. In the optimization studies, it was determined as 1000 μM in molecules **1** and **3**, and 500 μM in molecules **2** and **4**. XTT (2,3-bis-(2-methoxy-4-nitro-5-sulfophenyl)-2H-tetrazolium-5-carboxanilide) is a tetrazolium-based compound used for the colorimetric detection of viable mammalian cells. Following the manufacturer's instructions, 50 μL of XTT solution was added to each well and incubated for 4 h at 37 °C. The absorbance was then measured using an ELISA reader (BIOTEK, USA). XTT assay was repeated three times.

2.5. Wound healing assay

The analyses were carried out to determine metastatic ability [39]. Approximately 2×10^5 cells were added to each well in a 12-well plate. After one day, the cells covered 80 % of the well bottom. A vertical wound was quickly created in the monolayer using a 10 μL pipette tip. The cells were then washed with 1 mL of PBS to remove dead cells, followed by the addition of fresh medium and the molecules (**1-4**). Photographs were taken at 24–48 h to assess whether the molecules affected cell migration. Wound Healing assay was repeated three times.

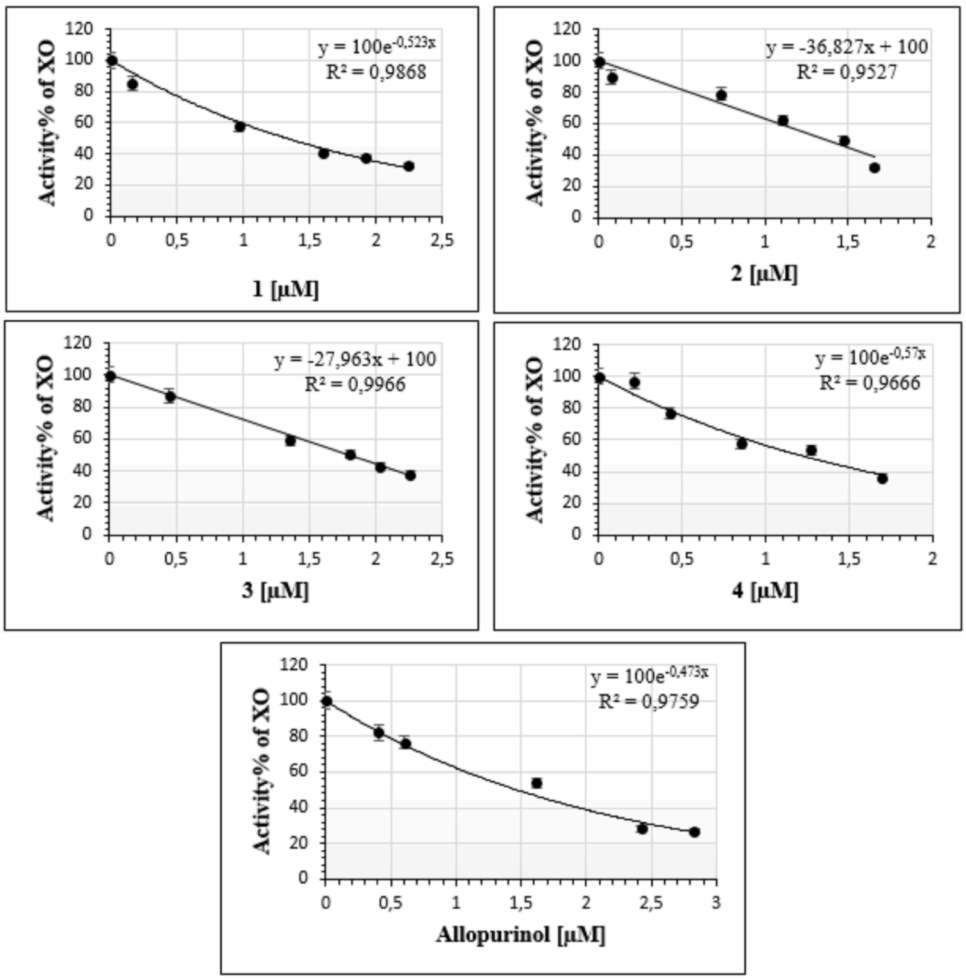

Fig. 3. The %Activity/ [Inhibitor concentration] graphs of the non-proteogenic amino acid derivatives (**1**-**4**) and allopurinol on XO activity.

2.6. ADME and druglikeness analyses

ADME and druglikeness analyses of the molecules were performed using the PKCSM (https://biosig.lab.uq.edu.au/pkcsm/) and SwissADME (https://www.swissadme.ch/) databases.

2.7. Molecular docking studies

Molecular docking evaluations were conducted to explore the interactions between non-proteinogenic amino acid compounds (**1, 2, 3, 4**) and XO using Induced-Fit Docking (IFD) simulations [40], as outlined in our previous work [41–45]. These simulations were carried out with Maestro 13.9, part of the Schrödinger Molecular Modeling Suite [46]. The XO crystal structure (PDB ID 3NVY) was retrieved from the RCSB Protein Data Bank, and the receptor was generated at physiological pH using the Protein Preparation Wizard [47], followed by optimization and minimization with force field the OPLS4. The receptor grid was created around the natural ligand to establish the binding site, while the LigPrep module was employed to protonate the ligands at a pH of 7.0 ± 2.0, ensuring their ionization states were optimized for biological relevance.

2.8. Binding free energy calculation via Molecular Mechanics/ Generalized Born Surface Area (MM-GBSA)

The binding free energies (ΔG_{bind}) were computed using the MM-GBSA (Molecular Mechanics/Generalized Born Surface Area) approach, a technique that combines molecular mechanics force fields with implicit solvation models to provide an efficient and accurate estimation of the binding affinities for protein-ligand complexes. Specifically, the Prime/MM-GBSA protocol was applied, leveraging the VSGB (Variable Dielectric Generalized Born) solvation model to account for solvent effects and the OPLS4 (Optimized Potentials for Liquid Simulations 4) force field to describe molecular interactions, as referenced in [48]. This approach enables a robust evaluation of binding energetics while balancing computational efficiency and accuracy.

2.9. Molecular dynamics simulations

Molecular dynamics simulations were executed with Desmond software, developed by D.E. Shaw Research, to study the behavior of the protein-ligand complex. Based on the molecular docking results, the compound with the highest binding affinity to the XO enzyme was selected and then incorporated into the enzyme structure. The protein-ligand complex was constructed using the system builder module in Desmond, which enabled the precise assembly and central positioning of the complex within an orthorhombic simulation box. To ensure sufficient solvation space, a 10 Å buffer zone was established around the protein. The system was then solvated using the Tip3p water model to replicate a realistic aqueous environment, and counter ions (NaCl at a concentration of 0.15 M) were incorporated to neutralize the system and approximate physiological ionic conditions. This configuration resulted in a fully solvated and charge-neutralized environment, ideal for conducting molecular dynamics simulations. The system was subjected to energy minimization using the OPLS4 force field to optimize the atomic coordinates and eliminate steric clashes. Following this, the complex

was imported into the Desmond molecular dynamics module, where a 250 ns simulation was performed under isothermal-isobaric conditions, maintaining a constant temperature of 300 K and a pressure of 1 bar, utilizing default simulation parameters to ensure consistency and reproducibility. The simulation was carried out with a time step of 2.5 fs, using the RESPA integrator for efficient time-stepping in the system. Detailed analysis was performed to assess the interactions between the ligand and the protein throughout the binding process, including the stability and nature of the ligand-protein complex. Additionally, the RMSD (Root Mean Square Deviation) of the protein's Cα atoms and the heavy atoms of the ligand were computed to track structural fluctuations and conformational changes over time. These measurements, obtained using Desmond, provided insights into the stability of both the protein and ligand during the simulation and their dynamic behavior within the complex.

2.10. Statistics analyses

BM SPSS 29 program was used for statistical analysis. The control group and other treated groups were analyzed. Nonparametric "Mann Whitney U" test was used and $P<0.05$ were considered statistically significant.

3. Results and discussion

Hyperuricemia is an important topic in medical science today. XO inhibitors are the primary target in drug design studies for the treatment of hyperuricemia-related disorders, especially gout [49,50]. Amino acid derivatives are one of the important compound groups that attract attention in prodrug development studies as enzyme inhibitors in the field of medicinal chemistry due to their important chemical properties [30–34]. In the present study, given the therapeutic significance of both XO inhibitors and amino acid derivatives, the inhibition effects of some non-proteonegenic amino acid derivatives on XO activity were examined. Inhibition studies were supported by molecular docking and molecular dynamics studies. Many studies indicate that there is a close relationship between cancer and hyperuricemia. For this reason, in this study, the cytotoxic effects of non-proteogenic amino acid derivatives, whose inhibition effect on XO activity was investigated, on triple-negative breast cancer cell lines (MDA-MB-231) were also investigated. Additionally, ADME analyzes of the molecules were also performed.

3.1. Inhibition effects of non-proteonegenic amino acid derivatives (1, 2, 3 and 4) on XO

The inhibitory effects of non-proteonegenic amino acid derivatives (**1, 2, 3** and **4**) on XO activity was quantitatively assessed by calculating their IC_{50} values, which represent the concentration of each inhibitor required to reduce the enzymatic activity by 50 %. While determining the IC_{50} values showing the inhibitory effects of **1, 2, 3, 4** compounds and allopurinol on XO activity, activity measurements were performed by adding at least five different concentrations of **1, 2, 3, 4** compounds and allopurinol to the reaction medium in XO activity measurement. The measurement without inhibitor was used as a control. All measurements were repeated three times under the same conditions. As a result of the measurements, Activity% versus inhibitor concentration graphs were drawn and IC_{50} values were determined using the equations of these graphs. For XO, IC_{50} values of molecules **1-4** were found to be 1.338 μM, 1.357 μM, 1.788 μM, 1.228 μM, respectively. Allopurinol was used as the reference inhibitor for XO (IC_{50}: 1.479 μM). Low IC_{50} value indicates a strong inhibitory effect. Based on the experimental findings, compound **4** exhibited the most persuasive inhibitory activity contra xanthine oxidase (XO), exhibiting the highest efficacy in suppressing enzymatic activity compared to the other tested compounds. When the inhibition results were matched with allopurinol, molecules **1, 2** and **4** showed a more effective inhibition effect than allopurinol, while the inhibition effect of molecule **3** was lower than allopurinol. The %Activity/[inhibitor concentration] graphs of the molecules (**1-4**) are shown in Fig. 3 and the inhibition results are summarized in Table 1.

Table 1
Inhibition results of non-proteogenic amino acid derivatives (**1-4**) on XO activity.

Compounds	IC_{50}
1	1.338 μM
2	1.357 μM
3	1.788 μM
4	1.228 μM
Allopurinol*	1.479 μM

* Allopurinol was used as reference inhibitor for XO

Table 2
IFD docking scores and Prime/MM-GBSA free binding energy results for the **1-4** compounds against the target receptor.

	XO	
Compound	IFD Docking Score (kcal/mol)	MM-GBSA ΔG_{bind} (kcal/mol)
1	-10.687	-36.00
2	-14.983	-60.27
3	-10.089	-79.90
4	-10.674	-69.96
Allopurinol*	-7.464	-17.55

* Allopurinol was used as reference inhibitor for XO

3.2. Molecular docking studies

We utilized the Induced-Fit Docking (IFD) procedure to management comprehensive molecular docking studies with **1-4** compounds to elucidate the protein-ligand interactions. These compounds, known for their potent inhibitory effects on the XO, were subjected to the IFD protocol. Allopurinol, a well-established XO enzyme inhibitor, served as the positive control. Furthermore, we employed Prime MM-GBSA module to gage the binding free energies, thereby gaining a deeper understanding of the thermodynamic parameters involved in the inhibition of XO by the **1-4** compounds. Table 2 provides a summary of the IFD docking scores and Prime/MM-GBSA values.

Molecular docking studies on the **1-4** compounds, which exhibited potent inhibitory effects against the XO enzyme in experimental *in vitro* assays, revealed substantially high docking scores and MM/GBSA free binding energies. In contrast, *in silico* studies for Allopurinol, the positive control, did not align with the experimental findings. This discrepancy is likely due to the relatively small chemical structure of Allopurinol, resulting in limited interaction with the enzyme's active site. Docking scores can vary significantly depending on the software, crystal structure, and docking protocol used. So, a wide range of docking scores for Allopurinol against the XO enzyme has been reported in the literature. For instance, in a study by Ghallab et al. using the Extra Precision (XP) protocol with the XO crystal structure 3NVY, the docking score for Allopurinol was reported as -4.975 kcal/mol [51]. Kikiowo et al. reported a docking score of -9.003 kcal/mol using the Induced-Fit Docking (IFD) protocol with the XO crystal structure 1FIQ [52]. Malik et al. found a docking score of -3.366 kcal/mol using the XP protocol with the XO crystal structure 2E1Q [53], while Nguyen et al. reported a docking score of -5.9 kcal/mol using the XP protocol with the XO crystal structure 1N5X [54]. Although it is challenging to make a direct comparison across these studies due to differences in methodology, our results align most closely with those of Kikiowo et al. [52], whose study employed a similar protocol to ours.

Although the IC_{50} values for the molecules examined for *in vitro*

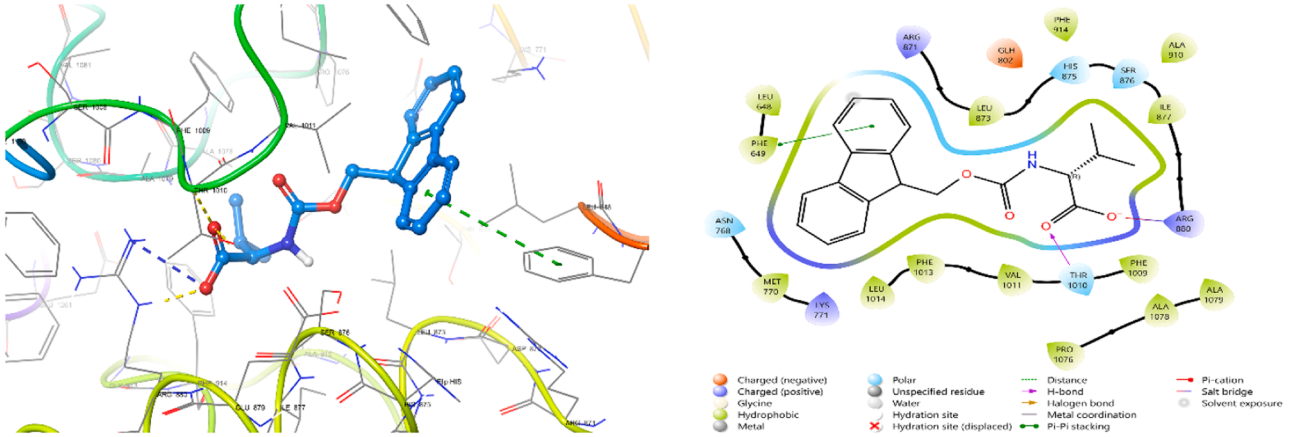

Fig. 4. The left panel displays the detailed 3D docking pose of compound **2** with the XO receptor, while the right panel presents the corresponding 2D ligand-receptor interaction diagram.

inhibition of the XO enzyme did not show significant differences, the compound **4** exhibited the strongest effect. Molecular docking studies supported this experimental data consistently. Both the docking score and the free binding energy of **4** were notably high. IFD simulations showed a striking docking score of -10.674 kcal/mol against the XO enzyme, reflecting a strong and favorable binding interaction between compound **4** and the enzyme. The subsequent MM-GBSA analysis calculated a free binding energy of -69.96 kcal/mol, further emphasizing the stability and strength of the interaction between compound **4** and XO (Table 2). Within the active site of the XO, compound **4** formed key hydrogen bonds with GLH802 and SER876, crucial residues that contribute to the enzyme's binding pocket. Additionally, compound **4** hooked in dual pi-pi stacking coactions with the aromatic residues PHE914 and PHE1009, which are vital to the structural integrity and catalytic activity of the active site. These interactions suggest a highly stable and specific binding of compound **4** to XO, which is likely to play a significant role in modulating its enzymatic function (Fig. S1). Although compound **4** exhibited the lowest experimental inhibitory effect, it did not demonstrate the most affirmative activity in terms of docking scores and binding energies. In silico data are typically used to validate experimental findings and predict inhibition mechanisms within the context of inhibition studies. Therefore, the high docking score and favorable binding energy of compound **4** are largely consistent with our experimental results.

Molecular docking studies on **1**, which demonstrated a potent experimental inhibition effect against the XO enzyme, further validated the experimental results. IFD simulations resulted a high docking score of -10.687 kcal/mol for the XO enzyme, indicating strong binding affinity. Additionally, MM/GBSA evaluations revealed a estimated binding free energy of -36.00 kcal/mol between **1** and the XO enzyme

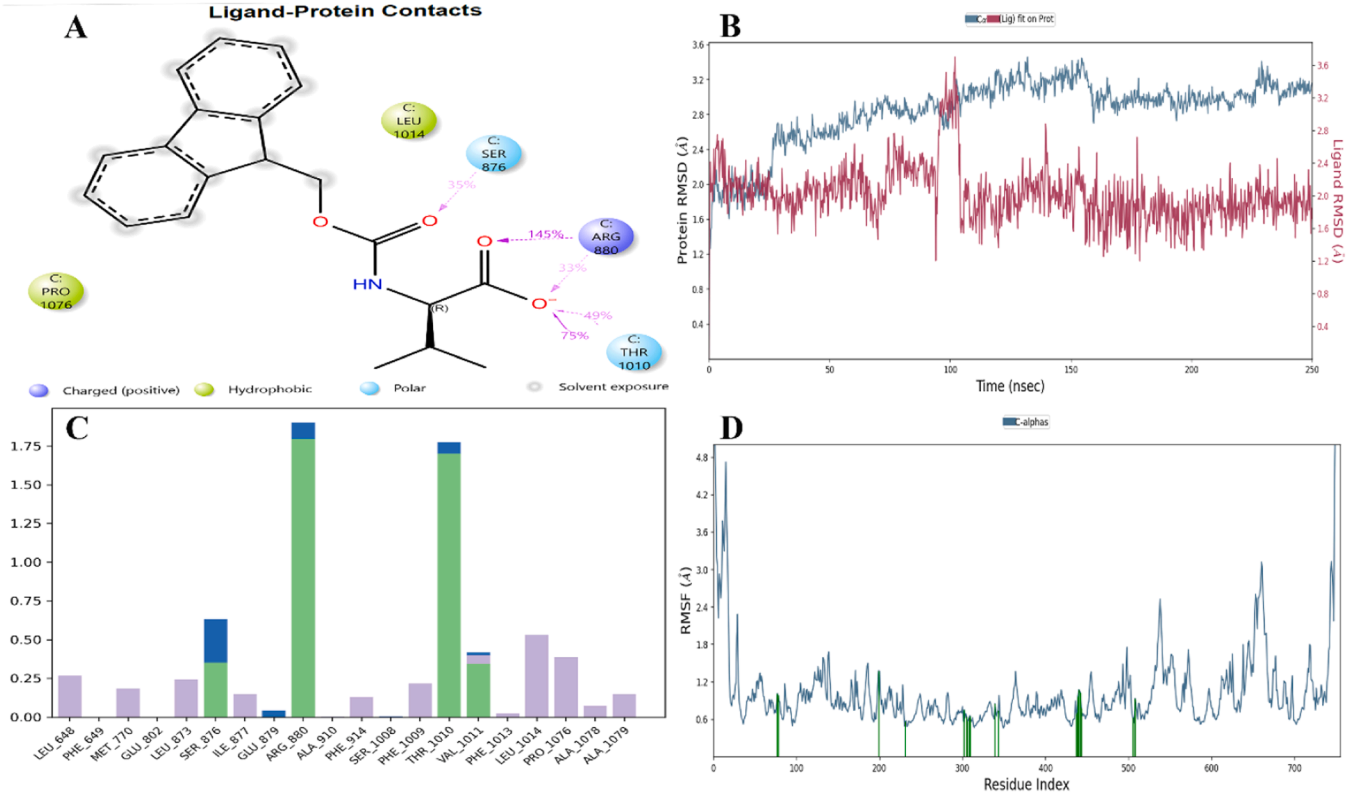

Fig. 5. Graphs depicting protein-ligand contacts (A), protein and ligand RMSD (B), protein-ligand interactions (C), and RMSF (D) for the compound **2**.

Table 3
3D structures of molecules **1-4**, IC_{50} values of molecules **1-4** on MDA-MB-231 cell line and XTT assay well images of the molecules **1-4**.

Molecules	3D structures of molecules	IC_{50} value (μM)	XTT assay
1	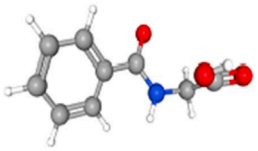	101.19	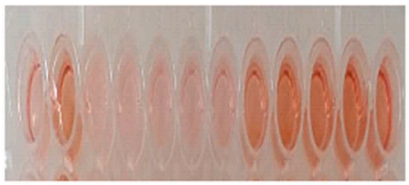
2	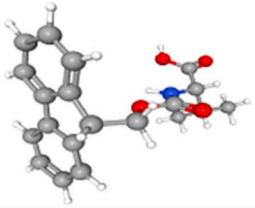	98.55	
3	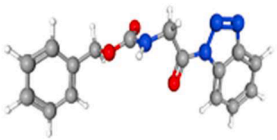	177	
4	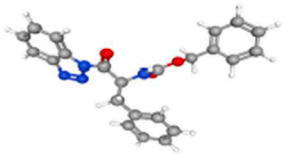	125	

(Table 2). **1** formed dual hydrogen bonds with the THR1010 residue and engaged in a salt bridge interaction with ARG880 in the active site of the XO enzyme (Fig. S2).

For the compound **2**, which exhibited a curiously potent inhibitory effect on the XO enzyme, computational studies further confirmed the empirical results. IFD simulations yielded exceptionally high docking scores of -14.983 kcal/mol for the XO, demonstrating a highly favorable and strong binding affinity between compound **2** and the enzyme. Following this, MM/GBSA evaluations provided computed binding free energies of -60.27 kcal/mol, further reinforcing the significant and stable interactions between compound **2** and XO (Table 2). This combination of results indicates a robust and energetically favorable binding interaction, suggesting that compound **2** forms a highly stable complex with the XO enzyme. **2** engaged in pi-pi interaction with PHE649, and constructed a hydrogen bond with THR1010, as well as a salt bridge with ARG880 within active site of the XO enzyme (Fig. 4).

Among the compounds studied for their inhibitory effects on XO enzymes **3** showed the lowest effect, even lower than the positive control compound Allopurinol. It was determined to have the lowest docking score in molecular docking studies. However, The MM-GBSA free binding energy for this compound deviated from experimental data, indicating discrepancies in computational predictions. IFD simulations resulted a docking score of -10.089 kcal/mol for the XO, while MM-GBSA analysis estimated a binding free energy of -79.90 kcal/mol (Table 2). Compound **3** formed hydrogen bonds with GLH802, ARG880, GLU1261, and THR1010, stabilizing its interaction within the binding pocket. Additionally, pi-pi stacking with PHE914 and PHE1009 reinforced its positioning in the active site (Fig. S3), highlighting key molecular interactions influencing its binding affinity.

Non-proteoneogenic amino acid derivatives and allopurinol showed very similar inhibitory activity in experimental studies, primarily interact with common residues in the active site of the XO enzyme. The standard inhibitor allopurinol interacted with GLH802, ARG880, SER876, and PHE914 amino acid residues in the active site of the XO enzyme (Fig. S4). All of the non-proteoneogenic amino acid derivatives were observed to interact with at least one of these amino acid residues (The most active compound, compound **4**, interacted with amino acids GLH802, SER876, and PHE914 in common with allopurinol). Therefore, it can be concluded that the GLH802, ARG880, SER876, and PHE914 amino acid residues play a key role in the inhibition of the XO enzyme.

While the carboxylic acid group of these derivatives consistently interacts with residues in the enzyme's active site, other functional groups within the compounds also participate in additional interactions, particularly pi-pi interactions. This complexity makes it challenging to establish a direct correlation between the structural features of these compounds and their docking activities.

3.3. *Molecular dynamics studies*

Although docking offers a fixed depiction of a molecule's binding orientation within a protein's active site, molecular dynamics (MD) simulations offer a dynamic perspective by calculating the movements of atoms over time using Newton's classical equations of motion [55]. To investigate the structural stability of the ligand/protein complex and

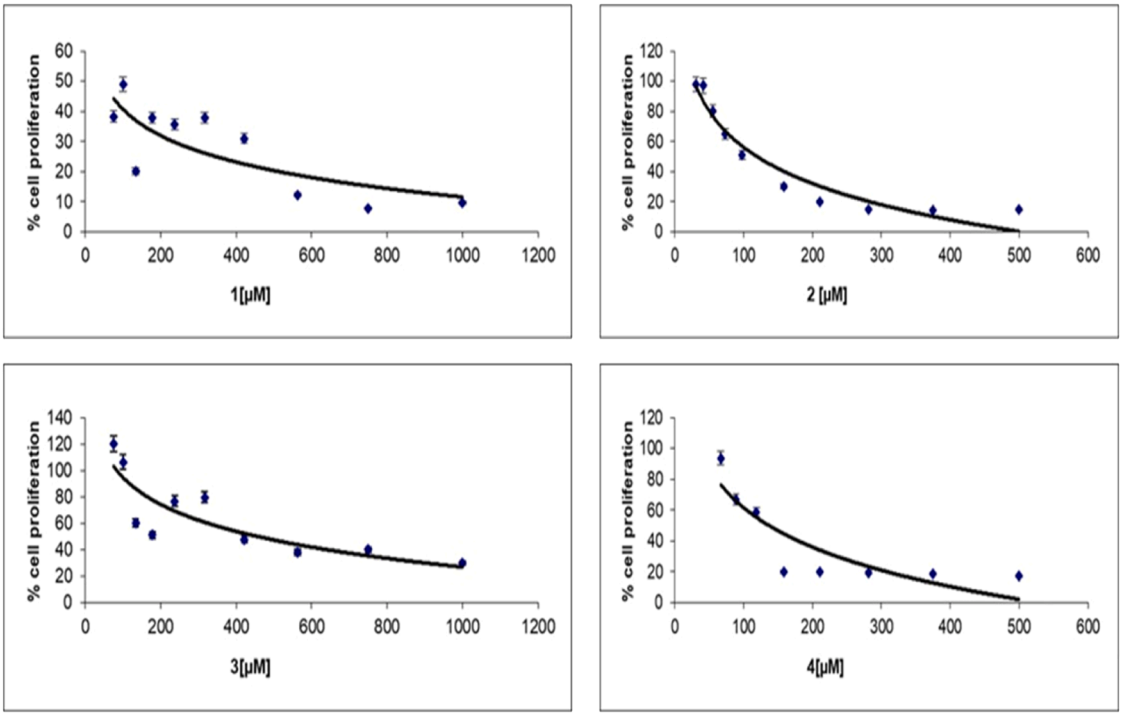

Fig. 6. The cytototoxicity analyses graphs of molecules (**1-4**).

elucidate the essential molecular interactions, MD simulations were carried out for compound **2**. This compound was selected due to the highest docking score, its excellent *in vitro* inhibition, and significant MM/GBSA binding free energy results. Fig. 5 depicts the outcomes of the MD simulation for the complex formed between the compound **2** and the XO enzyme.

Fig. 5A highlights critical ligand-protein contacts, where key residues such as ARG880, THR1010, and SER876 form predominant polar and charged interactions, contributing significantly to the binding stability. ARG880 stands out with its high interaction frequency (145 %), indicative of its strong electrostatic and hydrogen-bonding contributions to anchoring the ligand. Meanwhile, THR1010 (75 %) and SER876 (35 %) complement these interactions, reinforcing the ligand's orientation and reducing its degrees of freedom. The hydrophobic residues, including LEU1014 and PRO1076, further stabilize the ligand within the hydrophobic regions of the binding pocket, ensuring tight packing and reducing solvent exposure.

The RMSD analysis in Fig. 5B demonstrates the overall stability of the protein-ligand complex throughout the 250 ns simulation. The protein's Cα RMSD stabilizes around 2.5–3.0 Å after initial fluctuations, indicating that the global structure remains consistent, with no significant conformational deviations. The ligand's RMSD remains relatively low, below 1.5 Å, which strongly suggests that the ligand maintains a stable binding pose within the pocket throughout the simulation. The tight ligand RMSD reflects its resilience against external perturbations and reinforces the hypothesis of strong binding affinity.

Fig. 5C quantifies the frequency of interactions for residues involved in ligand binding. ARG880 emerges as the dominant interacting residue, highlighting its central role in stabilizing the ligand. Other residues such as THR1010, SER876, and GLU879 contribute moderately, forming transient but supportive interactions that enhance the dynamic stability of the complex. This synergy between highly frequent and transient interactions demonstrates a robust binding mechanism, where both persistent and flexible interactions cooperate to stabilize the ligand.

The RMSF plot in Fig. 5D further elucidates the protein's dynamic behavior. Residues in the binding site exhibit minimal fluctuations, confirming their structural rigidity, which is critical for maintaining a stable ligand-binding environment. In contrast, residues in solvent-exposed regions (e.g., 500–700) display higher flexibility, as expected for loop regions and peripheral domains. The rigidity of the binding site, combined with the flexibility of non-essential regions, supports the protein's ability to securely bind the ligand while maintaining overall conformational adaptability.

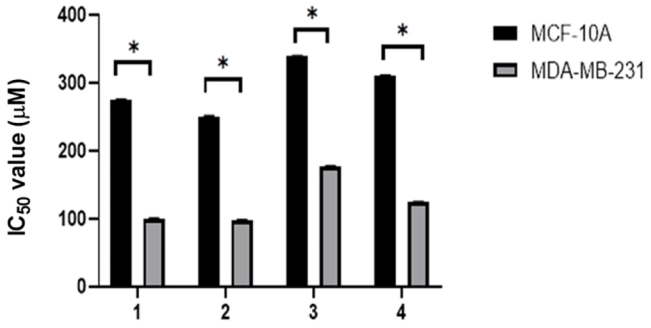

Fig. 7. The cytototoxicity analyses graphs of MDA-MB-231 and MCF-10A cells.

In conclusion, the molecular dynamics simulations reveal that the compound **2** forms a highly stable complex with xanthine oxidase, driven by strong polar and hydrophobic interactions with critical residues such as ARG880, THR1010, and SER876. The ligand demonstrates minimal deviation from its binding pose, reflecting strong affinity and stable engagement with the enzyme.

3.4. Cytotoxic effect of non-proteonegenic amino acid derivatives (1, 2, 3 and 4) on MDA-MB-231 and MCF-10A cell lines

3D structures, IC_{50} values and XTT assay well images of the molecules are given in Table 3. The IC_{50} values of the molecules in the cytotoxicity tests were determined as 101.19 μM, 98.55 μM, 177 μM and 125 μM for molecules **1-4**, respectively. According to the results obtained, it is seen that the effect of the 2nd molecule is more toxic on the cells than the others (Fig. 6). In this study, the toxic effects of non-

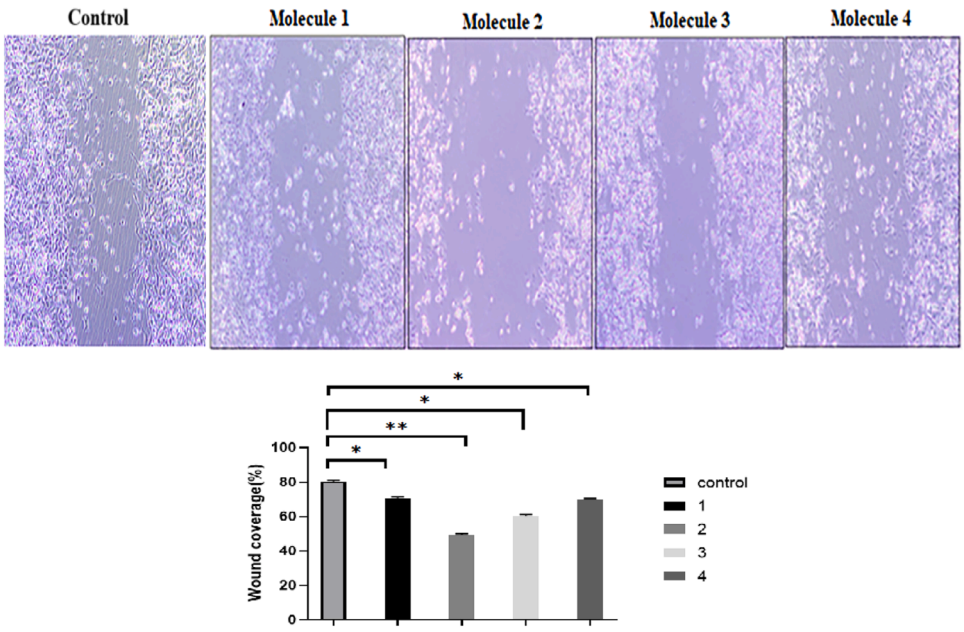

Fig. 8. Wound healing assay: application of control, 1st molecule, 2nd molecule, 3rd molecule, 4th moelcule in MDA-MB-231 cell lines (10X) (48 h) (* $p < 0.05$).

proteogenic amino acid derivatives (**1, 2, 3**, and **4**) were evaluated for cytotoxicity on the non-cancerous cell line MCF-10A. The results showed that the IC_{50} values of these compounds ranged from 250 to 340 μM, respectively. Statistical analysis of the results is presented in Fig. 7. The IC_{50} value for these molecules on MCF-10A cells was found to be greater than 250 μM, indicating low toxicity, while the dose required to kill 50 % of cancer cells was lower. Yuan et al. (2018) studied the toxic impact of non-protein amino acid derivatives on colon and gastric cancer cells. They synthesized 13 derivatives of 25-OCH3-PPD (compounds 1–13) and 12 derivatives of 25-OH-PPD (compounds 14–25) and evaluated their effects on HCT-116 and BGC-823 cancer cell lines using an MTT assay [56]. Their results showed that derivatives with IC_{50} values greater than 100 μM on cancer cells had little to no effect or demonstrated weak activity. Similarly, Rupar et al. (2020) investigated the effects of new 9-acridinyl amino acid derivatives on K562 and A549 cancer cell lines, as well as the normal diploid MRC5 cell line, and provided a comparative analysis of the toxic effects on these cells [57]. From the current study, we can conclude that molecule **2** demonstrates the best anti-tumor activity among the derivatives tested.

As shown in Fig. 8, cells treated with molecules were compared with untreated cells (control group). In Fig. 8, no molecule was treated to the cells (control group). The level of closure of the wound formed in the control group at 48 h was examined. It is seen that the wound is about to close at 48 h. Fig. 8 shows the cells to which molecules (**1-4**) were treated. At this stage, cell seeding and penetration were performed and molecules **1-4** were applied to the wound at the IC_{50} dose determined for each molecule by cytotoxicity analysis. Then the cells were photographed. According to the results obtained, it was observed that especially molecule **2** significantly inhibited cell migration in MDA-MB-231 cells compared to the untreated control (Fig. 8).

3.5. ADMET properties of non-proteonegenic amino acid derivatives (1, 2, 3 and 4)

An evaluation of the drug-likeness and ADMET properties of the molecules (**1-4**) was conducted to determine their suitability for oral use and pharmacological applications (Figs. S5–S8) [58–61].

Lipinski's Rule of Five (RO5), along with Egan's, Ghose's, Veber's, and Muegge's rules, serve as critical frameworks in drug discovery, assessing the drug-likeness of novel compounds based on physicochemical properties such as molecular weight, lipophilicity, and hydrogen bonding [58]. Evaluating drug-likeness is crucial in early-stage drug development, and the SwissADME tool (http://www.swissadme.ch/) was employed to determine the oral bioavailability of the selected compounds.

According to RO5, a compound is considered drug-like if it meets the following criteria: no more than 10 hydrogen bond acceptors (HBAs), no more than 5 hydrogen bond donors (HBDs), molecular weight (MW) $\leq$ 500 Da, and a log P value of ≤ 5, with only one deviation permitted [62]. All examined compounds adhered to these criteria. To further assess their absorption efficiency in the human body, a Bioavailability Radar was used [55,63]. As depicted in Fig. 9, this analysis visually represents bioavailability parameters, where the pink region denotes the optimal range [64,65]. Notably, only the second molecule entirely falls within this region, suggesting its bioavailability properties align well with drug-like characteristics, enhancing its potential for efficient absorption [66].

Table 4 confirms that all selected compounds comply with Lipinski's, Ghose's, and Veber's rules, reinforcing their suitability as drug candidates. However, Molecule 1 violated Muegge's rule due to its molecular weight falling below the acceptable threshold (MW $<$ 200), whereas Muegge's filter stipulates a range of 200 $\leq$ MW $\leq$ 600 [67]. The evaluation further demonstrated that molecules 1–4 met essential drug-likeness parameters, reinforcing their potential as viable drug candidates. Their bioavailability score of 0.55 further suggests they exhibit favorable bioavailability.

To refine their pharmacokinetic profiles, additional screening was conducted, including PAINS (Pan Assay Interference Compounds) alerts and synthetic accessibility (SA) evaluation. None of the molecules triggered PAINS alerts, confirming their potential as viable drug leads. Their synthetic accessibility scores were recorded as 3.57, 2.75, and 3.64 for molecules 2, 3, and 4, respectively (Table 4), indicating moderate synthetic feasibility.

ADMET predictions encompassed P-glycoprotein substrate status, human intestinal absorption (HIA), CNS distribution, blood-brain barrier (BBB) permeability, interactions with cytochrome P450 enzymes (CYP), AMES toxicity, total clearance, and hERG inhibition. The HIA values, ranging from 92 % to 95 %, suggest strong absorption potential through the intestinal membrane, whereas compounds with HIA values below 30 % are considered poorly absorbed. Molecules 2, 3, and 4

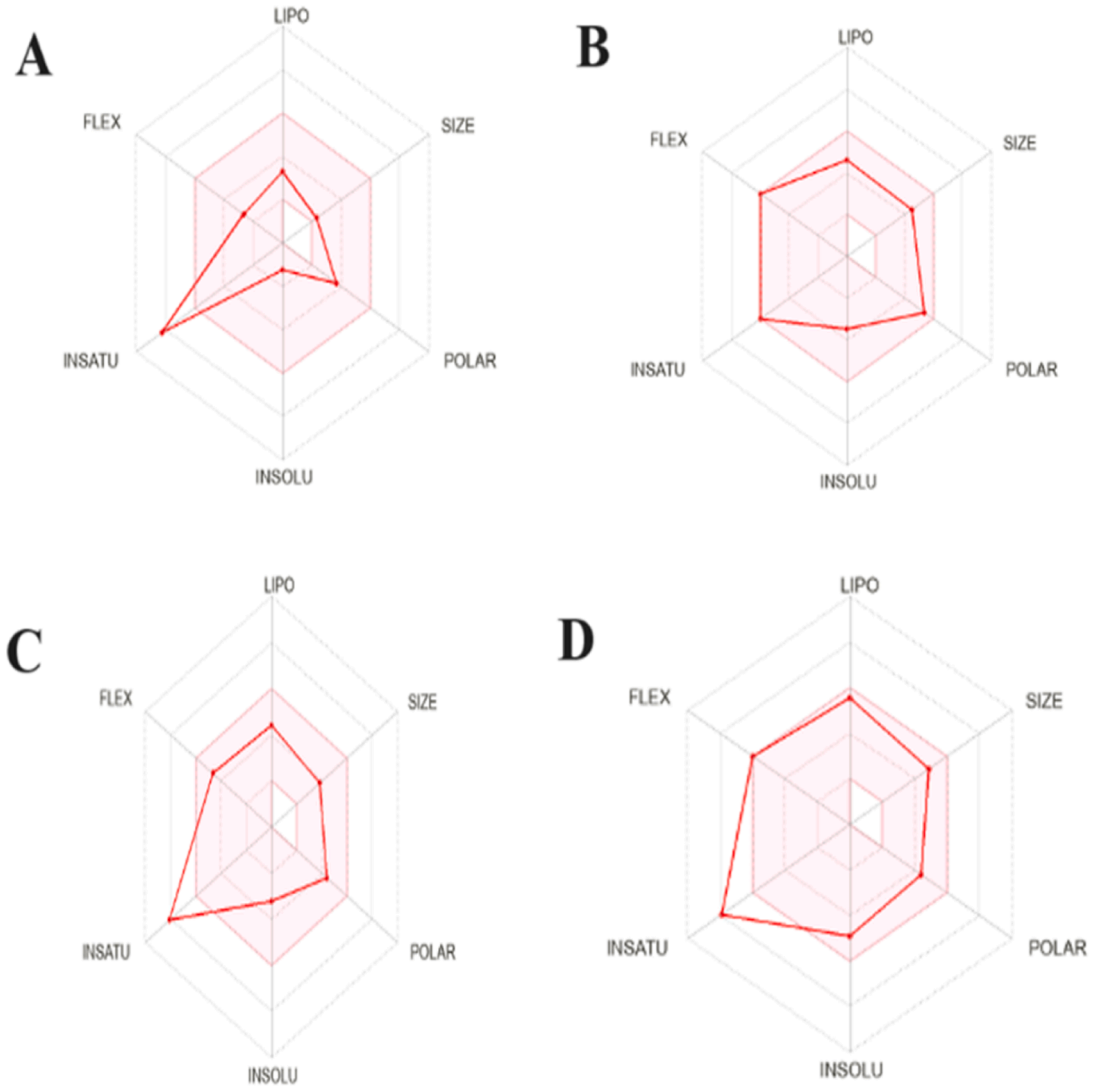

Fig. 9. The Radar charts of Molecules (**1-4**) (A: 1st molecule, B: 2nd molecule, C: 3rd molecule, D: 4th molecule) http://www.swissadme.ch/index.php.

Table 4
Evaluation of drug-likeness of molecules (**1-4**) (http://www.swissadme.ch/index.php#).

Molecules	Lipinski's Parameters *										
	MW(≤500Da)	MlogP(≤5)	HBA(≤10)	HBD(≤5)	Ghose	Veber	Egan	Muegge	B/A score	PAINS	SA
1	179.17 g/mol	0.84	3	2	Yes	Yes	Yes	No (1 violation MW<200)	0.85	0	1
2	369.37 g/mol	1.90	6	3	Yes	Yes	Yes	Yes	0.56	0	3.57
3	310.31 g/mol	2.24	5	1	Yes	Yes	Yes	Yes	0.55	0	2.75
4	400.43g/mol	3.62	5	1	Yes	Yes	Yes	Yes	0.55	0	3.64

* MW: molecular weight; HBA: hydrogen bond acceptor; HBD: hydrogen bond donor; B/A: bioavailability score; SA: synthetic accessibility; PAINS: Pan Assay Interference Compounds

displayed HIA values above 92 %, highlighting their favorable absorption profiles. Toxicity assessments further confirmed that none of the molecules exhibited skin sensitization or hERG I inhibition, reinforcing their safety profile.

4. Conclusion

The fact that hireuricemia is closely associated with many pathological conditions, including cancer, especially gout, that XO inhibitors are central to the control of hyperuricemia, and that existing XO inhibitors have life-threatening side effects, makes the issue of identifying new XO inhibitors important. In this study, considering the close relationship between hyperuricemia and cancer, the inhibition effects of **1-4** non-proteogenic amino acid derivatives on XO activity and their cytotoxic effects on breast cancer were examined together. The study was supported by molecular docking and molecular dynamics and ADME analyses. When the inhibition effects of amino acids **1-4** on XO activity were compared with the reference inhibitor of XO, allopurinol, it was seen that molecules **1, 2** and **3** exhibited better inhibition effects than alloprinol, and molecules **4** had an inhibition effect close to allopurinol. When looking at the cytotoxic effect of the molecules on MDA-MB-231 cell lines, it was observed that all molecules **1-4** had a cytotoxic effect

on MDA-MB-231 cell lines and the **2**nd molecule showed a stronger toxic effect than the other molecules. In conclusion, we hope that the data obtained in this study will contribute to the synthesis of new, effective and fewer side effects amino acid-derived XO inhibitors in the design of XO inhibitor drugs for the treatment of hyperuricemia.

CRediT authorship contribution statement

Zuhal Alım: Writing – review & editing, Writing – original draft, Visualization, Validation, Supervision, Resources, Methodology, Investigation, Formal analysis, Data curation, Conceptualization. **Serap Yalçın Azarkan:** Writing – review & editing, Resources, Methodology, Investigation. **Namık Kılınç:** Writing – review & editing, Visualization, Resources, Methodology. **Ebru Akkemik:** Writing – review & editing, Validation.

Declaration of competing interest

No potential conflict of interest was reported by the authors.

Supplementary materials

Supplementary material associated with this article can be found, in the online version, at doi:10.1016/j.molstruc.2025.142497.

References

[1] S. Wang, X. Liu, Z. He, X. Chan, W. Liet, Hyperuricemia has an adverse impact on the prognosis of patients with osteosarcoma, Tumour Biol. 37 (2016) 1205–1210, https://doi.org/10.1007/s13277-015-3830-3.

[2] H.K. Choi, D.B. Mount, A.M. Reginato, Pathogenesis of gout, Ann. Intern. Med. 143 (2005) 499–516, https://doi.org/10.7326/0003-4819-143-7-200510040-00009.

[3] A. Mehmood, M. Ishaq, L. Zhao, B. Safdar, A. Rehman, M. Munir, A. Raza, M. Nadeem, W. Iqbal, C. Wang, Natural compounds with xanthine oxidase inhibitory activity: a review, Chem. Biol. Drug Des. 93 (2019) 387–418, https://doi.org/10.1111/cbdd.13437.

[4] E. Krishnan, Interaction of inflammation, hyperuricemia, and the prevalence of hypertension among adults free of metabolic syndrome: NHANES 2009–2010, J. Am. Heart Assoc. 3 (2014) e000157, https://doi.org/10.1161/JAHA.113.000157.

[5] D. Gustafsson, R. Unwin, The pathophysiology of hyperuricaemia and its possible relationship to cardiovascular disease, morbidity and mortality, BMC Nephrol. 14 (2013) 164, https://doi.org/10.1186/1471-2369-14-164.

[6] Mm. Chen, Lh. Meng, The double faced role of xanthine oxidoreductase in cancer, Acta Pharmacol. Sin. 43 (2022) 1623–1632, https://doi.org/10.1038/s41401-021-00800-7.

[7] M. Maciejczyk, M. Nesterowicz, A. Zalewska, G. Biedrzycki, P. Gerreth, K. Hojan, K. Gerreth, Salivary xanthine oxidase as a potential biomarker in stroke diagnostics, Front. Immunol. 13 (2022) 897413, https://doi.org/10.3389/fimmu.2022.897413.

[8] M.A. Fini, A. Elias, R.J. Johnson, R.M. Wright, Contribution of uric acid to cancer risk, recurrence, and mortality, Clin. Transl. Med. 1 (2012) 16, https://doi.org/10.1186/2001-1326-1-16.

[9] Z. Jin, X. Feng, D. Wang, Y. Zhu, J. Liang, H. Zhang, J. Zhao, L. Sun, Global, regional and national trends in sex-and age-specific disability-adjusted life years of musculoskeletal disorders, 1990-2019, Rheumatology 61 (2022) 2978–2986, https://doi.org/10.1093/rheumatology/keab804.

[10] M. Rouquette, S. Page, R. Bryant, M. Benboubetra, C.R. Stevens, D.R. Blake, W. D. Whish, R. Harrison, D. Tosh, Xanthine oxidoreductase is asymmetrically localised on the outer surface of human endothelial and epithelial cells in culture, FEBS Lett. 426 (1998) 397–401, https://doi.org/10.1016/s0014-5793(98)00385-8.

[11] P. Higgins, J. Dawson, M. Walters, The potential for xanthine oxidase inhibition in the prevention and treatment of cardiovascular and cerebrovascular disease, Cardiovasc. Psychiatry Neurol. (2009) 282059, https://doi.org/10.1155/2009/282059, 2009.

[12] D.A Kostic, D.S. Dimitrijevic, G.S. Stojanovic, I.R. Palic, A.S. Dordevic, J. D. Ickovski, Xanthine oxidase: isolation, assays of activity, and inhibition, J. Chem. (2015) 294858, https://doi.org/10.1155/2015/294858, 2015.

[13] M. Martorell, X. Lucas, P. Alarcón-Zapata, X. Capó, M.M. Quetglas-Llabrés, S. Tejada, A. Sureda, Targeting xanthine oxidase by natural products as a therapeutic approach for mental disorders, Curr. Pharm. Des. 27 (2021) 367–382, https://doi.org/10.2174/1381612826666200621165839.

[14] P. Ebrahimpour, H. Fakhrzadeh, R. Heshmat, F. Bandarian, B. Larijani, Serum uric acid levels and risk of metabolic syndrome in healthy adults, Endocr. Pract. 14 (2008) 298–304, https://doi.org/10.4158/EP.14.3.298.

[15] H.M. Schmidt, E.E. Kelley, A.C. Straub, The impact of xanthine oxidase (XO) on hemolytic diseases, Redox Biol. 21 (2019) 101072, https://doi.org/10.1016/j.redox.2018.101072.

[16] Y. Xie, P. Xu, K. Liu, S. Lin, M. Wang, T. Tian, C. Dai, Y. Deng, N. Li, Q. Hao, L. Zhou, Z. Dai, H. Guo, Hyperuricemia and gout are associated with cancer incidence and mortality: a meta-analysis based on cohort studies, J. Cell Physiol. 234 (2019) 14364–14376, https://doi.org/10.1002/jcp.28138.

[17] M.S. Rahaman, M.A. Siraj, M.A. Islam, P.C. Shanto, O. Islam, M.A. Islam, J. Simal-Gandara, Crosstalk between xanthine oxidase (XO) inhibiting and cancer chemotherapeutic properties of comestible flavonoids- a comprehensive update, J. Nutr. Biochem. 110 (2022) 109147, https://doi.org/10.1016/j.jnutbio.2022.109147.

[18] A.F.G. Cicero, F. Fogacci, R.I. Cincione, G. Tocci, C. Borghi, Clinical effects of xanthine oxidase inhibitors in hyperuricemic patients, Med. Princ. Pract. 30 (2021) 122–130, https://doi.org/10.1159/000512178.

[19] M. Gliozzi, N. Malara, S. Muscoli, V. Mollace, The treatment of hyperuricemia, Int. J. Cardiol. 213 (2016) 23–27, https://doi.org/10.1016/j.ijcard.2015.08.087.

[20] A. Mehmood, L. Zhao, C. Wang, M. Nadeem, A. Raza, N. Ali, A.A. Shah, Management of hyperuricemia through dietary polyphenols as a natural medicament: a comprehensive review, Crit. Rev. Food Sci. Nutr. 59 (2019) 1433–1455, https://doi.org/10.1080/10408398.2017.1412939.

[21] J. Gao, X. Liu, B. Zhang, Q. Mao, Z. Zhang, Q. Zou, X. Dai, S. Wang, Design, synthesis and biological evaluation of 1-alkyl-5/6-(5-oxo-4,5- dihydro-1,2,4-oxadiazol-3-yl)-1H-indole-3-carbonitriles as novel xanthine oxidase inhibitors, Eur. J. Med. Chem. 190 (2020) 112077, https://doi.org/10.1016/j.ejmech.2020.112077.

[22] R. Kumar, G. Joshi, H. Kler, S. Kalra, M. Kaur, R. Arya, Toward an understanding of structural insights of xanthine and aldehyde oxidases: an overview of their inhibitors and role in various diseases, Med. Res. Rev. 38 (2018) 1073–1125, https://doi.org/10.1002/med.21457.

[23] A. Smelcerovic, K. Tomovic, Z. Smelcerovic, Z. Petronijevic, G. Kocic, T. Tomasic, Z. Jakopin, M. Anderluh, Xanthine oxidase inhibitors beyond allopurinol and febuxostat; an overview and selection of potential leads based on in silico calculated physico-chemical properties, predicted pharmacokinetics and toxicity, Eur. J. Med. Chem. 135 (2017) 491–516, https://doi.org/10.1016/j.ejmech.2017.04.031.

[24] P. Pacher, A. Nivorozhkin, C. Szabo, Therapeutic effects of xanthine oxidase inhibitors: renaissance half a century after the discovery of allopurinol, Pharmacol. Rev. 58 (2006) 87–114, https://doi.org/10.1124/pr.58.1.6.

[25] W.B. White, K.G. Saag, M.A. Becker, J.S. Borer, P.B. Gorelick, A. Whelton, B. Hunt, M. Castillo, L. Gunawardhana, Cardiovascular safety of febuxostat or allopurinol in patients with gout, N. Engl. J. Med. 378 (2018) 1200–1210, https://doi.org/10.1056/NEJMoa1710895.

[26] F.H. Messerli, M. Burnier, Cardiovascular disease and uric acid: is the not-soinnocent bystander becoming a true culprit and does the US black box warning for febuxostat indicate that not all uric acid lowering is beneficial? Eur. Heart J. 40 (2019) 1787–1789, https://doi.org/10.1093/eurheartj/ehz199.

[27] S. Oyama, C. Hirose, K. Hori, K. Sugano, J. Zhang, M. Tamura, K. Tomita, Effects, safety, and plasma levels of topiroxostat and its metabolites in patients receiving hemodialysis, Ren. Replace Ther. 2 (2016) 56, https://doi.org/10.1186/s41100-016-0068-5.

[28] M. Sakuma, T. Toyoda, T. Arikawa, Y. Koyabu, T. Kato, T. Adachi, H. Suwa, J. Narita, K. Anraku, K. Ishimura, F. Yamauchi, Y. Sato, T. Inoue, Topiroxostat versus allopurinol in patients with chronic heart failure complicated by hyperuricemia: a prospective, randomized, open-label, blinded-end-point clinical trial, PLoS One 17 (2022) e0261445, https://doi.org/10.1371/journal.pone.0261445.

[29] B. Zhang, X. Dai, Z. Bao, Q. Mao, Y. Duan, Y. Yang, S. Wang, Targeting the subpocket in xanthine oxidase: design, synthesis, and biological evaluation of 2-[4-alkoxy-3-(1H-tetrazol-1-yl) phenyl]-6-oxo-1,6-dihydropyrimidine-5- carboxylic acid derivatives, Eur. J. Med. Chem. 181 (2019) 111559, https://doi.org/10.1016/j.ejmech.2019.07.062.

[30] K.H. Park, M.J. Kurth, Cyclic amino acid derivatives, Tetrahedron 58 (2002) 8629–8659, https://doi.org/10.1016/S0040-4020(02)00989-4.

[31] K. Fosgerau, T. Hoffmann, Peptide therapeutics: current status and future directions, Drug Discov. Today 20 (2015) 122–128, https://doi.org/10.1016/j.drudis.2014.10.003.

[32] M.A.T. Blaskovich, Unusual amino acids in medicinal chemistry, J. Med. Chem. 59 (2016) 10807–10836, https://doi.org/10.1021/acs.jmedchem.6b00319.

[33] S.S. Katiyar, V. Kushwah, C.P. Dora, R.Y. Patil, S. Jain, Design and toxicity evaluation of novel fatty acid-amino acid-based biocompatible surfactants, AAPS PharmSciTech 20 (2019) 186, https://doi.org/10.1208/s12249-019-1396-x.

[34] B.L. De Sausa, J.P. Leite, T.A. De Oliveira Mendes, E.V.V. Varejao, A.C.S. Chaves, J. G. Silva, A.P. Agrizzi, P.G. Ferreira, E. Pilau, E. Silva, M.H. Dos Santos, Inhibition of acetylcholinesterase by coumarin-linked amino acids synthetized via triazole associated with molecule partition coefficient, J. Braz. Chem. Soc. 32 (2021) 652–664, https://doi.org/10.21577/0103-5053.20200219.

[35] F. Zhu, E. Miller, W.C. Powell, K. Johnson, A. Beggs, G.E. Evenson, M.A. Walczak, Umpolung AlaB reagents for the synthesis of non-proteogenic amino acids, peptides and proteins, Angew. Chem. Int. Ed. 61 (2022) e202207153, https://doi.org/10.1002/anie.202207153.

[36] J. Welsh, Animal models for studying prevention and treatment of breast cancer, in: P. Michael Conn (Ed.), Animal Models for the Study of Human Disease, Academic Press, USA, 2013, pp. 997–1018. https://doi.org/10.1016/B978-0-12-415894-8.00040-3.

[37] D.L. Holliday, V. Speirs, Choosing the right cell line for breast cancer research, Breast Cancer Res. 13 (2011) 215, https://doi.org/10.1186/bcr2889.
[38] V. Massey, P.E. Brumby, H. Komai, G. Palmer, Studies on milk xanthine oxidase: some spectral and kinetic properties, J. Biol. Chem. 244 (1969) 1682–1691, https://doi.org/10.1016/S0021-9258(18)91738-2.
[39] J.Y. Kim, T.T.P. Dao, K. Song, S.B. Park, H. Jang, M.K. Park, S.U. Gan, Y.S. Kim, *Annona muricata* leaf extract triggered intrinsic apoptotic pathway to atten- uate cancerous features of triple negative breast cancer MDA-MB-231 cells, Evid. Based Complement. Altern. Med. (2018) 7972916, https://doi.org/10.1155/2018/7972916, 2018.
[40] W. Sherman, T. Day, M.P. Jacobson, R.A. Friesner, R. Farid, Novel procedure for modeling ligand/receptor induced fit effects, J. Med. Chem. 49 (2006) 534–553, https://doi.org/10.1021/jm050540c.
[41] A. Akıncıoğlu, S. Göksu, A. Naderi, H. Akıncıoğlu, N. Kılınç, İ. Gülçin, Cholinesterases, carbonic anhydrase inhibitory properties and in silico studies of novel substituted benzylamines derived from dihydrochalcones, Comput. Biol. Chem. 94 (2021) 107565, https://doi.org/10.1016/j.compbiolchem.2021.107565.
[42] Z. Alım, H. Şirinzade, N. Kılınç, E. Dilek, S. Süzen, Assessing indole derivative molecules as dual acetylcholinesterase and butyrylcholinesterase inhibitors through *in vitro* inhibition and molecular modelling studies, J. Mol. Struct. 1311 (2024) 138276, https://doi.org/10.1016/j.molstruc.2024.138276.
[43] N. Gök, A. Akıncıoğlu, E.Erümit Binici, H. Akıncıoğlu, N. Kılınç, S. Göksu, Synthesis of novel sulfonamides with anti-Alzheimer and antioxidant capacities, Arch. Pharm. 354 (2021) e2000496, https://doi.org/10.1002/ardp.202000496 (Weinheim).
[44] N. Kılınç, M. Açar, S. Tuncay, Ö.F. Karasakal, Identification of potential inhibitors for severe acute respiratory syndrome-related Coronavirus 2 (SARS-CoV-2) angiotensin-converting enzyme 2 and the main protease from anatolian traditional plants, Lett. Drug Des. Discov. 19 (2022) 996–1006, https://doi.org/10.2174/1570180819666211230123145.
[45] N. Kılınç, U. Güller, Z. Alım, Identification of the inhibition effects of some natural antiproliferative agents on CA-I, CA-II, and AChE activities isolated from human erythrocytes by kinetic and molecular docking studies, Russ. J. Bioorg. Chem. 48 (2022) 720–730, https://doi.org/10.1134/S1068162022040124.
[46] Schrödinger Release 2024–1: Maestro, Schrödinger, LLC, New York, NY 2024.
[47] G.M. Sastry, M. Adzhigirey, T. Day, R. Annabhimoju, W. Sherman, Protein and ligand preparation: parameters, protocols, and influence on virtual screening enrichments, J. Comput. Aided Mol. Des. 27 (2013) 221–234, https://doi.org/10.1007/s10822-013-9644-8.
[48] S. Genheden, U. Ryde, The MM/PBSA and MM/GBSA methods to estimate ligand-binding affinities, Expert Opin. Drug Discov. 10 (2015) 449–461, https://doi.org/10.1517/17460441.2015.1032936.
[49] S. Pang, Q. Jiang, P. Sun, Y. Li, Y. Zhu, J. Liu, X. Ye, T. Chen, F. Zhao, W. Yang, Hyperuricemia prevalence and its association with metabolic disorders: a multicenter retrospective real-world study in China, Ann. Transl. Med. 9 (2021) 1550, https://doi.org/10.21037/atm-21.
[50] N. Otani, M. Ouchi, E. Mizuta, A. Morita, T. Fujita, N. Anzai, I. Hisatome, Dysuricemia-a new concept encompassing hyperuricemia and hypouricemia, Biomedicines 11 (2023) 1255, https://doi.org/10.3390/biomedicines11051255.
[51] D.S. Ghallab, E. Shawky, A.M. Metwally, I. Celik, R.S. Ibrahim, M.M. Mohyeldin, Integrated *in silico–in vitro* strategy for the discovery of potential xanthine oxidase inhibitors from Egyptian propolis and their synergistic effect with allopurinol and febuxostat, RSC Adv. 12 (2022) 2843–2872, https://doi.org/10.1039/d1ra08011c.
[52] B. Kikiowo, A.J. Ogunleye, O.K. Inyang, N.S. Adelakun, O.I. Omotuyi, D. S. Metibemu, T.T. Ijatuyi, Flavones scaffold of chromolaena odorata as a potential xanthine oxidase inhibitor: induced fit docking and ADME studies, Bioimpacts 10 (2020) 227–234, https://doi.org/10.34172/bi.2020.29.
[53] N. Malik, P. Dhiman, A. Khatkar, In silico design and synthesis of targeted rutin derivatives as xanthine oxidase inhibitors, BMC Chem. 13 (2019) 1–13, https://doi.org/10.1186/s13065-019-0585-8.
[54] H.T. Nguyen, T.Y. Vu, T.C. Dakal, B. Dhabhai, X.H.Q. Nguyen, V.B. Tatipamula, Cleroda-4 (18), 13-dien-15, 16-olide as novel xanthine oxidase inhibitors: an integrated *in silico* and *in vitro* study, PLoS One 16 (6) (2021) e0253572, https://doi.org/10.1371/journal.pone.0253572.
[55] S.A. Adcock, J.A. McCammon, Molecular dynamics: survey of methods for simulating the activity of proteins, Chem. Rev. 106 (2006) 1589–1615, https://doi.org/10.1021/cr040426m.
[56] W. Yuan, J. Guo, X. Wang, G. Su, Y. Zhao, Non-protein amino acid derivatives of 25-methoxylprotopanaxadiol/25-hydroxyprotopanaxadioland their anti-tumour activity evaluation, Steroids 129 (2018) 1–8, https://doi.org/10.1016/j.steroids.2017.11.003.
[57] J. Rupar, V. Dobričić, J. Grahovac, S. Radulović, Ž. Skok, J. Ilaš, M. Aleksić, J. Brborić, O. Čudina, Synthesis and evaluation of anticancer activity of new 9-acridinyl amino acid derivatives, RSC Med. Chem. 11 (2020) 378–386, https://doi.org/10.1039/c9md00597h.
[58] A. Daina, O. Michielin, V. Zoete, SwissADME: a free web tool to evaluate pharmacokinetics, drug-likeness and medicinal chemistry friendliness of small molecules, Sci. Rep. 7 (2017) 42717, https://doi.org/10.1038/srep42717.
[59] D.E.V. Pires, T.L. Blundell, D.B. Ascher, pkCSM: predicting small-molecule pharmacokinetic and toxicity properties using graph-based signatures, J. Med. Chem. 58 (2015) 4066–4072, https://doi.org/10.1021/acs.jmedchem.5b00104.
[60] A.B. Umar, A. Uzairu, G.A. Shallangwa, S. Uba, In silico evaluation of some 4-(quinolin-2-yl) pyrimidin-2-amine derivatives as potent V600E-BRAF inhibitors with pharmacokinetics ADMET and drug-likeness predictions, Future J. Pharm. Sci. 6 (2020) 61, https://doi.org/10.1186/s43094-020-00084-4.
[61] A.I. Foudah, M.H. Alqarni, A. Alam, M.A. Salkini, S.A. Ross, H.S. Yusufoglu, Phytochemical screening, *in vitro* and *in silico* studies of volatile compounds from petroselinum crispum (Mill) leaves grown in Saudi Arabia, Molecules 27 (2022) 934, https://doi.org/10.3390/molecules27030934.
[62] C.A. Lipinski, F. Lombardo, B.W. Dominy, P.J. Feeney, Experimental and computational approaches to estimate solubility and permeability in drug discovery and development q settings, Adv. Drug Deliv. Rev. 23 (1997) 3–25, https://doi.org/10.1016/S0169-409X(96)00423-1.
[63] A. Rauf, H. Khan, M. Khan, A. Abusharha, G. Serdaroğlu, M. Daglia, *In silico*, SwissADME, and DFT studies of newly synthesized oxindole derivatives followed by antioxidant studies, J. Chem. 2023 (2023) 5553913, https://doi.org/10.1155/2023/5553913.
[64] M. Abdul-Hammed, I.O. Adedotun, M. Olajide, C.O. Irabor, T.L. Afolabi, I. O. Gbadebo, L. Rhyman, P. Ramasami, Virtual screening, ADMET profiling, PASS prediction, and bioactivity studies of potential inhibitory roles of alkaloids, phytosterols, and flavonoids against COVID-19 main protease (Mpro), Nat. Prod. Res. 36 (2022) 3110–3116, https://doi.org/10.1080/14786419.2021.1935933.
[65] O.M. Alshehri, A. Zeb, S.M. Mukarram Shah, M.H. Mahnashi, S.A. Asiri, O. Alqahtani, A. Sadiq, M. Ibrar, S. Alshamrani, M.S. Jan, Investigation of anti-nociceptive, anti-inflammatory potential and ADMET studies of pure compounds isolated from Isodon rugosus Wall. ex Benth, Front. Pharmacol. 15 (2024) 1328128, https://doi.org/10.3389/fphar.2024.1328128.
[66] C. Jaafaru, A. Uzairu, M.S. Sallau, G.I. Ndukwe, M.T. Ibrahim, K. Tabti, P. Kandpal, V. Kumar, *In-silico* exploration and structure-based design of Praziquantel derivatives as potential inhibitors of schistosoma mansoni Glutathione S-transferase (SmGST), Sci. Afr. 24 (2024) e02169, https://doi.org/10.1016/j.sciaf.2024.e02169.
[67] I. Muegge, S.L. Heald, D. Brittelli, Simple selection criteria for drug-like chemical matter, J. Med. Chem. 44 (2001) 1841–1846, https://doi.org/10.1021/jm015507e.